ACS Photonics

pubs.acs.org/journal/apchd5

Article

Large-Area Transparent "Quantum Dot Glass" for Building-Integrated Photovoltaics

Jing Huang, Jingjian Zhou, Erik Jungstedt, Archana Samanta, Jan Linnros, Lars A. Berglund, and Ilya Sychugov*

Cite This: *ACS Photonics* 2022, 9, 2499–2509

Read Online

ACCESS | Metrics & More | Article Recommendations | Supporting Information

ABSTRACT: A concept of transparent "quantum dot glass" (TQDG) is proposed for a combination of a quantum dot (QD)-based glass luminescent solar concentrator (LSC) and its edge-attached solar cells, as a type of transparent photovoltaics (TPVs) for building-integrated photovoltaics (BIPVs). Different from conventional LSCs, which typically serve as pure optical devices, TQDGs have to fulfill requirements as both power-generating components and building construction materials. In this work, we demonstrate large-area (400 cm^2) TQDGs based on silicon QDs in a triplex glass configuration. An overall power conversion efficiency (PCE) of 1.57% was obtained with back-reflection for a transparent TQDG (average visible transmittance of 84% with a color rendering index of 88 and a low haze ≤3%), contributing to a light utilization efficiency (LUE) of 1.3%, which is among the top reported TPVs based on the LSC technology with similar size. Most importantly, these TQDGs are shown to have better thermal and sound insulation properties compared to normal float glass, as well as improved mechanical performance and safety, which significantly pushes the TPV technology toward practical building integration. TQDGs simultaneously exhibit favorable photovoltaic, aesthetic, and building envelope characteristics and can serve as a multifunctional material for the realization of nearly zero-energy building concepts.

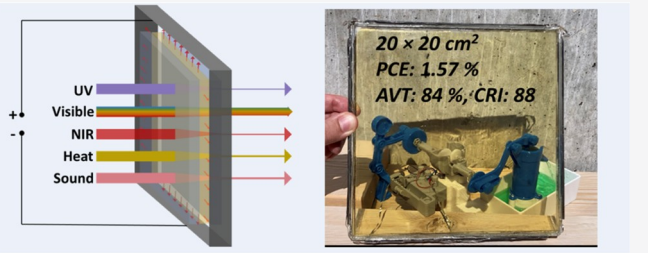

KEYWORDS: *quantum dot glass, photovoltaics, aesthetics, building envelope, silicon quantum dots, luminescent solar concentrator*

INTRODUCTION

Building-integrated photovoltaics (BIPV) technology, in which photovoltaic (PV) elements are integrated into building envelopes in the form of PV skins or glazing units, can be central to realize the goal of the zero-energy buildings (NZEBs). It is a rapidly growing research field, where concepts of transparent and colored photovoltaics, in particular, are gaining attraction.[1−6] The BIPV technology can be implemented in the window area, where conventional opaque PVs have limited coverage, as solar windows. Then, for application in real buildings, the parameter of average visible transmittance (AVT) becomes significant since aesthetics of the windows strongly influence their social acceptance and market penetration.[3,5,7−9] Transparent photovoltaics (TPVs), with optimized AVT and power conversion efficiency (PCE), offer an exciting approach to fabricate solar windows. TPVs can be realized by several kinds of technologies, for instance, segmenting opaque PV cells[10,11] or utilizing a sufficiently thin light-absorbing film, such as for organic photovoltaics (OPV)[12−14] and perovskite PV,[15,16] to increase the AVT of these devices. However, the high cost and complexity of large-area fabrication, as well as low aesthetics with strong color tints, still greatly limit their further commercialization.[3,12]

Another attractive solution is a combination of a luminescent solar concentrator (LSC) with edge-mounted PV cells over its perimeter.[4,6,17−19] The LSC is an optical device devised in the 1970s to reduce the area of then-expensive solar cells.[20−22] Fluorophores in an LSC (organic dyes,[23−26] quantum dots,[27−35] perovskite nanocrystals,[36−38] metal nanoclusters,[39,40] etc.) are responsible for light harvesting with fluorescence waveguided to the edges by total internal reflection (TIR). For the conventional LSCs, their main objective is to concentrate light to the greatest extent, and thus "concentration ratio" is a significant parameter.[41,42] To enhance this figure of merit, LSCs can be fully absorbing, thus possessing strong color tints or high scattering.[26,28,43] For the same purpose, only one edge is often covered with solar cells and sometimes the rest with mirrors.[44,45] In addition, although several electrical PCE values are reported for LSCs as PV devices, a very small size solar cell is often coupled to a part

Received: April 27, 2022
Published: June 27, 2022

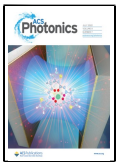

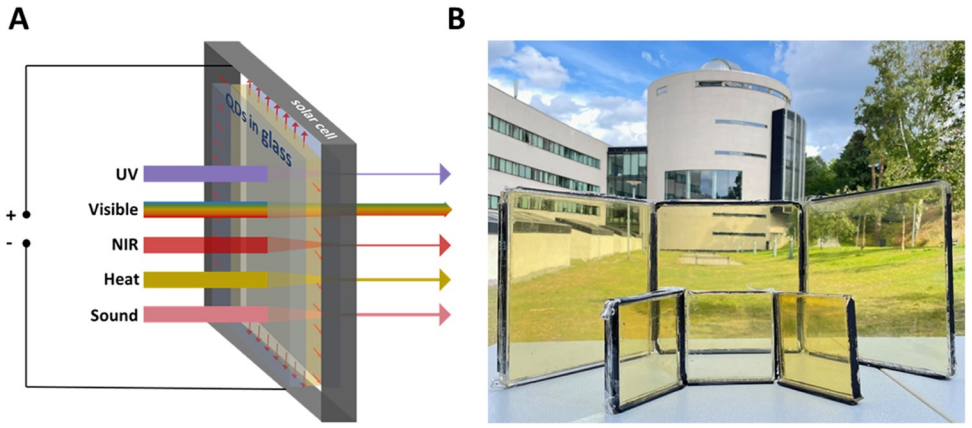

Figure 1. Concept of the TQDG and devices. Illustration of the TQDG concept (A) and demonstration of the fabricated TQDGs (B) in this work.

of the edge, which is not appropriate as a correct assessment for the overall PV device performance.[23,28] Clearly, pristine LSCs in their original meaning are not suitable for building-integrated TPVs, although applications as sound barriers, decorative panels, and curtain walls are sometimes considered.[46−49]

A different purpose as glazing units in BIPV will redefine device design and, hence, figure of merit. Here, a moderate light absorption and low haze are required since maintaining a high transmittance is an important requirement for solar windows. Second, as a figure of merit, the electrical PCE is more relevant to characterize it as a power generator, rather than as an optical device. Finally, the reported components need to be compatible with building envelope material requirements. In this work, we use a concept of transparent "quantum dot glass" (TQDG), where all of these characteristics are equally weighted to realize a multifunctional BIPV material.

Quantum dots have demonstrated promising properties as suitable fluorophores for solar windows due to their good stability, high photoluminescence quantum yield (PLQY), and suppressed reabsorption loss by a large Stokes shift.[27−33,50−53] In particular, Si QDs emerged as promising fluorophores for TQDG, attributed to nontoxicity, elemental abundance, large Stokes shift, and a high PLQY of emission in the near-infrared (NIR) region,[27,29,54−56] where low-cost synthesis is also available.[57] At the same time, the rich surface functionality of Si QDs offers good compatibility with different TQDG matrices.[43,58] Here, we rely on a triplex glass laminate configuration of TQDG, which provides good protection for the active interlayer[35] and enhances unit mechanical strength,[59,60] making it suitable to become a part of the building envelope.

For practical implementation as solar windows, only devices with large area (≥100 cm^2) are meaningful, no matter which technology is used for the fabrication of TPVs. Therefore, reporting photovoltaic performance and aesthetic parameters for large-area devices or modules is helpful for the real assessment of different technologies. Here, TQDGs with a surface area of 400 cm^2 have been fabricated, which can be applied directly or tiled into modules for BIPV applications. These TQDGs consist of a layer of Si QDs/polymer composite sandwiched between two pieces of glass. The photovoltaic performance of the devices was optimized by changing the thickness and QD loading of the composite interlayer, and the aesthetic quality was fully evaluated. As a result, a highly transparent (AVT of 84%) TQDG with good photovoltaic performance (PCE of 1.57% with a back-reflector) is demonstrated. Light utilization efficiency (LUE)[5] of this optimized TQDG is 1.3%, which is superior among reported TPVs based on the LSC technology with a similar size. At the same time, the color rendering index (CRI)[5] of such TQDG under the sun was 88, demonstrating visual comfort of a "warm" color with CIELAB coordinates (93, −4, 28), accompanied by a very low haze (≤3%). Furthermore, we show that favorable mechanical, heat, and sound insulation properties, superior to normal float glass, can be achieved for BIPV, without any deterioration of photovoltaic or aesthetic characteristics. Therefore, in this work, functionality, aesthetics, safety, and insulation property were all evaluated and balanced for PV windows of large area, demonstrating that the TQDG is very promising for practical implementation in building envelopes.

RESULTS AND DISCUSSION

TQDG Theory and Fabricated Devices. *Working Principle.* The TQDG mainly consists of two components: laminated glass with embedded QDs and edge-mounted PV cells, as illustrated in Figure 1A. QDs partially absorb incoming sunlight and re-emit it at longer wavelengths, which then propagates to the edges through TIR. Subsequently, the attached solar cells over the whole perimeter utilize fluorescence that reaches edges and convert it into electrical power. At the same time, for glazing function, visible light should be transmitted to a large extent (≥50%) without haze, while thermal and sound insulation, as well as the mechanical strength of the device, should comply with the characteristics of a building envelope material.[61−64] In Figure 1A, we introduce a general concept of the TQDG, which serves as a multifunctional building envelope material.

Following the working principle of the TQDG, its PCE value depends on QD properties, device geometry, as well as characteristics of the attached solar cells (for details, see Supporting Information 1, S1)

$$\mathrm{PCE} = \frac{eV_{oc}}{h\nu_{abs}} \cdot \mathrm{FF} \cdot \mathrm{EQE}_{cell} \cdot A_{QD} \cdot \mathrm{QY} \cdot \delta \cdot \eta_{wvgd} \quad (1)$$

where V_{oc}, FF, and EQE_{cell} are open-circuit voltage, fill factor, and external quantum efficiency of the attached solar cell, respectively; $h\nu_{abs}$ is an average energy of the absorbed photons, which is around 2.7 eV for the TQDG with Si QDs

https://doi.org/10.1021/acsphotonics.2c00633
ACS Photonics 2022, 9, 2499−2509

Table 1. Detailed Parameter Information of the Fabricated TQDGs

TQDG[a]	dimension (cm^2)	thickness of interlayer (mm)	effective amount of QDs (mg)	QD loading (wt %)[b]	A_{QD}
TQDG-*s*-3	9 × 9	3	5.1	0.017%	8.09%
TQDG-*s*-6	9 × 9	6	9.4	0.016%	10.2%
TQDG-*s*-6-H	9 × 9	6	23.7	0.040%	17.7%
TQDG-*l*-6	20 × 20	6	51.5	0.019%	11.3%
TQDG-*l*-6-H	20 × 20	6	74.6	0.027%	14.5%
TQDG-*l*-10	20 × 20	10	69.9	0.014%	12.8%
TQDG-*l*-no-QDs	20 × 20	6	0	0	

[a]"*s*", "*l*", and "H" in the device labels represent the small area, large area, and high loading of the devices, respectively, while the number refers to the thickness of the interlayer. [b]"QD loading, wt %" refers to the mass ratio of QDs in the interlayer.

(peak position of the absorbed photon spectrum); and δ is a waveguiding fraction (~75% for n = 1.5, which is unity minus escape cone losses of 25%). These factors are treated as constants here. A_{QD} is the fraction of the absorbed solar irradiance by QDs, which depends on the load of QDs;[32] η_{wvgd} is a waveguiding efficiency, which is one of the most important parameters in TQDG. For a square shape TQDG with a side length l, it can be evaluated as[65,66]

$$\eta_{wvgd} = \frac{M_1(2\alpha lk/\sqrt{\pi})\cdot\alpha\sqrt{\pi}}{\delta(\alpha_{sc} + QY\cdot\alpha_{re})(lk\alpha + M_1(2\alpha lk/\sqrt{\pi})\cdot\sqrt{\pi}) - lk\alpha^2} \quad (2)$$

where α [cm^{-1}] is the sum of scattering α_{sc} [cm^{-1}], reabsorption α_{re} [cm^{-1}], and matrix absorption α_{mx} [cm^{-1}] coefficients: $\alpha = \alpha_{sc} + \alpha_{re} + \alpha_{mx}$ (all have negligible wavelength dependence in the luminescence range of Si QDs); k is a coefficient for 3D geometry: $k \approx 1.14$ for n = 1.5; M_1 (ξ) is a modified Struve function of the second kind. eq 1 makes it possible to *a priori* evaluate the contribution of QD PL to the device efficiency directly from material and geometry parameters without numerical integration.

Equation 2 indicates that the device size plays a significant role in the waveguiding efficiency, which we explicitly demonstrate for Si QD TQDG by plotting η_{wvgd} (l) in Figure S1. In addition, it can also be influenced by the scattering coefficient, which is related to nanoparticle agglomeration and resulting polymer quality. The matrix absorption and reabsorption coefficients can be treated as constants here: 0.04 cm^{-1} for the glass/polymer absorption and 0.007 cm^{-1} for the Si QD reabsorption at this wavelength range.[27] So, for a given type of fluorophores, it is their load (A_{QD}, α_{sc}) and device geometry (l) that affect the PCE of the TQDG. In general, both AVT values and the size should be mentioned together with reported PCE values for TQDGs.[67,68]

An auxiliary quantity describing the wavelength-dependent response of the TQDG is an external quantum efficiency (EQE), which is a photon-to-electron conversion factor. Only those solar photons, which are absorbed ($A(\lambda)$), converted to luminescence (QY), emitted to the waveguiding mode (δ), and waveguided to the edges (η_{wvgd}), are detected

$$EQE(\lambda) = EQE_{cell}\cdot A(\lambda)\cdot QY\cdot\delta\cdot\eta_{wvgd} \quad (3)$$

where EQE_{cell} is the photon-to-electron conversion of the attached solar cell at the wavelength of QD emission.

Figures of Merit for the TQDG. As a BIPV technology, the TQDG should have a dual function of generating power and as construction materials for building envelopes. For power generation, as mentioned above, a size-dependent PCE value of the device should be reported for a fair comparison in different material systems. Simultaneously, the TQDG also should fulfill the requirements of aesthetical quality and mechanical and insulation properties. Employed as a window for the buildings, aesthetics of TQDG play a significant role in their public acceptance.[1,3,5,7−9] Normally, the aesthetical quality of TPVs is evaluated in three aspects: AVT, color rendering, and haze.[5,50]

Controlling AVT is important for both performance and aesthetics. Generally, a window with AVT >60% looks clear, while that with values <50% appears as dark, colored, and/or reflective.[5] Ideally, AVT ≥ 50% is preferable for TPVs to balance high transmittance and sizable absorption for electricity conversion. Recently, a new figure of merit, light utilization efficiency (LUE), was suggested for the comprehensive evaluation of the TPV quality,[5,12,19] including both PCE and AVT. It was defined as LUE = PCE × AVT and can also be applied in TQDGs for a better comparison between different technologies. For a PV window, this merit represents an overall system efficiency as a combination of power generation efficiency and light throughput (transmitted light per incident light power).[5] Nevertheless, in the practical comparison of different TQDG material systems, LUE should be compared for devices with the same dimension. Inclusion of these different practical aspects calls for a new figure of merit in reporting TPV prototypes beyond established optical and photovoltaic characterizations.

Fabricated Devices. As depicted in Figure S2A, the TQDGs studied in this work consist of a layer of the Si QD/polymer composite sandwiched between two pieces of glass, which were fabricated by directly pouring the QD/monomer mixture into a prepared glass box followed by polymerization with a UV LED (detailed in Supporting Information 1, S2b), and commercial monocrystalline silicon solar cells were then coupled to the edges (photovoltaic performance shown in Figure S4). Off-stoichiometric thiol−ene (OSTE), with a thiol/allyl group ratio of 2/1, was chosen as a polymer matrix for the TQDGs due to documented beneficial effects on PLQY enhancement and stability of Si QDs.[27,56,69,70] As shown in Figure S2B,C, the fluorescence of the synthesized Si QDs peaked around 850 nm, and the PLQY of the QD/OSTE matrix was 50−60%. A large Stokes shift (~400 nm) between absorption and fluorescence can be observed, resulting in a low reabsorption coefficient of 0.007 cm^{-1} for this material system.[27] Emission spectra from the edge of the TQDG (Figure S2D, Supporting Information 1, without solar cell attachment) show that there is almost no peak shift for the emission spectra with the excitation spot distance d, proving that the losses to reabsorption are indeed negligible. The NIR emission from Si QDs matches well with the high EQE region

https://doi.org/10.1021/acsphotonics.2c00633
ACS Photonics 2022, 9, 2499−2509

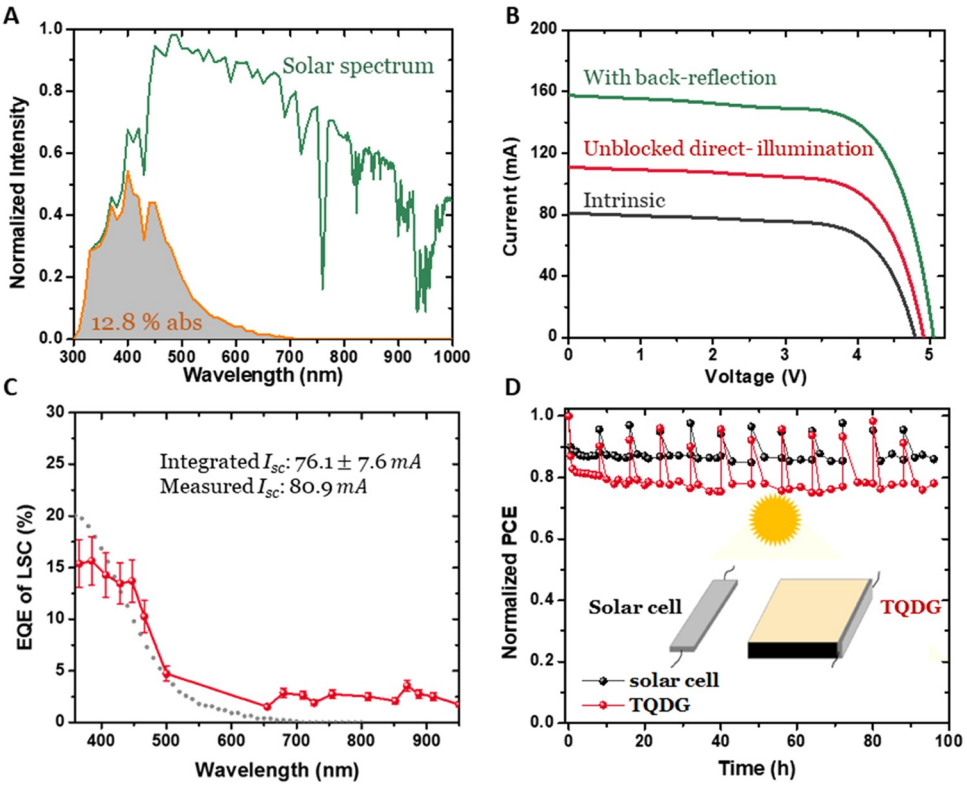

Figure 2. Photovoltaic performance of TQDGs. (A) Calculated solar absorption (orange) for TQDG-*l*-10 taken from the convolution of the solar spectrum (green) and the device absorption spectrum (green curve in Figure 3A). (B) *I*−*V* curves for TQDG-*l*-10 (with edges fully covered by solar cells) measured under different conditions: "intrinsic" as the standard measurement; the mask on the edges of the TQDG removed for measurements with unblocked direct illumination; and with a white paper as back-reflector and unblocked direct illumination. (C) Measured (red line) and theoretical (gray dots) EQE spectra of TQDG-*l*-10 (with edges fully covered by solar cells) measured as "intrinsic". (D) PV performance photostability data of the TQDG (TQDG-*s*-6-H, with one edge covered by a solar cell) and a separate solar cell placed side by side under AM1.5G irradiation.

(∼90%) of the attached silicon solar cells in TQDGs (Figure S4B).

In this work, we focused on the fabrication of TQDG prototypes with dimensions of 20 × 20 cm^2. For performance optimization, three smaller TQDGs with dimensions of 9 × 9 cm^2 were also made, as demonstrated in Figure 1B. The optimization was mainly carried out from varying QD loading and thickness of the interlayer, which can influence the absorbed fraction of the solar power A_{QD} and scattering coefficient in the devices, with detailed information summarized in Table 1.

From Table 1, one can find that the absorbed fraction of the solar power A_{QD} in TQDGs grows sublinearly with the amount of QDs. This fact implies that the utilization of QDs is less efficient for higher loads. To clarify this effect, we explicitly calculated the absorption fraction dependence on the Si QD load (Figure S5). From the convolution of the QD absorption spectrum with the solar irradiance (inset in Figure S5), we find that the absorption in the UV-blue region quickly saturates and then grows slowly in the visible range at higher QD loads. A similar phenomenon was reported in devices based on $CuInS_2$ QDs[50] and dyes.[71] Therefore, it is reasonable to select the load well below 350 mg (AVT ≈ 50% level) for Si QDs in a 20 × 20 cm^2 device. Such devices with a high AVT will also be free from saturated colors, which can be detrimental to aesthetical perception.

Photovoltaic Performance. *Power Conversion Efficiency.* To measure the intrinsic PCE of the TQDGs, the solar cells connected in parallel were attached to the devices covering all edges, unless specified otherwise. An opaque mask was applied on top of the solar cells to block direct illumination on them, following an established protocol.[67,68] Then, the TQDGs were placed under an LED-based AM1.5 G solar simulator (active area 25 × 25 cm^2) for standard current−voltage (*I*−*V*) measurements. Here, I_{sc} values are mainly reported for the devices, rather than J_{sc} values. The TQDG is not an ordinary PV cell, and it is designed to be used as a solar window. Therefore, ultimate generated power for a large-area device is a more relevant parameter. Moreover, due to the waveguiding effect, the overall I_{sc} from the whole device is not linearly related to the size, and the current density J_{sc} is less significant for TQDGs.

Calculated solar absorption and measured *I*−*V* curves of the smaller TQDGs (TQDG-*s* series) are presented in Figure S6, with detailed parameters summarized in Table S1. Haze at 800 nm, which can be interpreted as a scattering coefficient α_{SC} for the devices, slightly increased with a thicker interlayer and higher QD loading. However, the increment did not induce much difference in the calculated waveguiding efficiency of the TQDGs since the values were still too low to result in a significant impact for these small sizes. Nevertheless, it is worth noting that a high scattering will have a significant effect if the size is enlarged to 1 × 1 m^2.[27] Regarding *I*−*V* performance, the short circuit current, I_{sc}, proportionally increased with the absorbed sunlight fraction, as expected. Consequently, higher PCE was obtained for devices with a higher QD loading. Based

https://doi.org/10.1021/acsphotonics.2c00633
ACS Photonics 2022, 9, 2499−2509

on these results from small devices, we selected appropriate thicknesses and load values for large-area TQDGs, as summarized in Table 1.

The solar absorption fraction and $I-V$ curves of the TQDGs with 20 × 20 cm^2 (TQDG-*l* series) are shown in Figure S7, with related parameters summarized in Table S2. Similar to the smaller devices, large-area TQDG with higher absorption fraction delivered higher output power, resulting in a higher PCE. Due to the similar haze level of the TQDGs, waveguiding efficiencies of the large devices were close. However, it is noticeable that waveguiding efficiency was lower for the larger devices due to the size effect of the QD-LSC component, and hence, PCE values of larger TQDGs were lower than those from 9 × 9 cm^2 devices. Summarizing all of these results, when TQDGs are employed as BIPV windows, their photovoltaic performance is strongly influenced by the size and the absorption fraction of the solar power.

As mentioned above, to reveal the intrinsic PCE of the TQDGs, a mask was used to block direct illumination to the solar cells. However, in real situations, the sun is changing position during the day, and therefore, this direct exposure is inevitable and can in fact improve TQDG performance. To mimic this kind of situation, we also carried out $I-V$ characterization without a screen for direct illumination. As shown by the red curve in Figure 2B and Table 2, the I_{sc} increased by ∼30%, resulting in an enhanced PCE to 1.08% for the TQDG-*l*-10 device with edges fully covered by solar cells.

Table 2. Summarized PV Parameters from $I-V$ Measurements of TQDG-*l*-10 under Different Conditions

$I-V$ measurements for TQDG-*l*-10	I_{sc} (mA)	V_{oc} (V)	FF	number of edges covered by solar cells	PCE of TQDG (%)
intrinsic	80.9	4.81	0.79	4	0.77
unblocked direct illumination	110.9	4.92	0.79	4	1.08
with back-reflection and unblocked direct illumination	157.4	5.05	0.79	4	1.57

In addition to the direct illumination, back-reflection from the building interior, such as white walls, curtains, and doors, may also contribute. For a standard $I-V$ measurement for TQDGs, a black absorbing background was used to ensure a single optical pass through the semitransparent device. To quantify back-reflection effect, a white paper was used as the background, which can also be an approximation of the use of interior blinds or curtains to block sunlight. With the reflection and unblocked direct illumination, the current further increased, and, consequently, the PCE of the fully covered TQDG-*l*-10 device further improved to 1.57%. This large enhancement can be attributed to the low intrinsic absorption of the device, where the optical double pass induced by the white background can substantially increase the absorbed fraction. So, the performance of a highly transparent device can markedly benefit from the back-reflector, approaching the one with strong single-pass absorption under these conditions. Therefore, we have shown that in real conditions, the PCE of the TQDG-*l*-10 device can approach ∼1.5%. For tiled TQDGs with a dimension of 20 × 20 cm^2, the PCE of ∼1.5% translates to ∼15 W/m^2 of the electrical peak power, which can represent a sizable contribution to the net-zero-energy building concept.

External Quantum Efficiency. To elucidate different contributions to the intrinsic device efficiency, EQE measurements were carried out. Calculated EQE (λ) from eq 3 (gray dots) and measured EQE (λ) (red dots) of the TQDGs are displayed in Figures 2C and S8. For almost all of the TQDGs, the measured EQE values were consistent with the calculated ones in the range of Si QD absorption (400−650 nm). Yet, there were some deviations in the UV and red-to-NIR parts. For the former, the measured EQE values were generally slightly lower than the calculations predicted. In fact, a photoinitiator (Irgacure-184) was used here for device fabrication. It absorbs UV light, together with UV possible absorption by the OSTE polymer matrix (as manifested in Figure S9), thus competing in UV absorption with QDs, but generates no photoelectrons (Figure S8F). Note that the borosilicate glass used here does not absorb in the solar UV range. This negative effect was largely offset by EQE enhancement in the red-to-NIR region (650−1000 nm). For all of the TQDG devices, the measured EQE values in this region were higher than the calculated ones. The enhancement was higher for the devices with a higher haze (Figure S8A−C). EQE increment in this region can result from stray light from the solar simulator, reaching perimeter solar cells. It was shown that for small devices and moderate scattering the net effect on the efficiency can indeed be positive.[72] This might be the reason why the control TQDG sample without QDs also demonstrated a very faint power output (Figure S7B). However, this scattering effect can quickly become detrimental, as for the high-haze device TQDG-*s*-6-H, in which the measured EQE values are obviously lower than expected in the visible range (Figure S8C). Consequently, as a general rule, the haze of the TQDG must be kept at a very low level both for aesthetics and for performance. Based on these results, we can distinguish several contributions to the measured PCE value: QD PL (described by eq 1, 65%), scattered NIR light (>650 nm in Figure 2C; 35%), direct illumination (+40%), and the same contributions from the back-reflected light (+104% in the case of full back-reflection).

EQE measurements are not only useful in clarifying different inputs to the overall efficiency but can also provide an important consistency check for the short circuit current I_{sc}.[68] From Figure 2C, we can see that the calculated I_{sc} values from the integration of the spectrally resolved EQE measurements with solar spectrum (eq S8) matched well with the I_{sc} values directly obtained from $I-V$ curves under one sun irradiation, confirming the accuracy of the presented photovoltaic characterization.

Photostability. Photostability under AM1.5G condition was also tested for this type of TQDGs. A device (TQDG-*s*-6-H, with one edge covered by solar cells and the others painted black) and a solar cell was separately exposed to one sun for 100 hours in a day−night cycle. Their normalized PCE values are shown in Figure 2D. Results reveal that both the stand-alone solar cell and the TQDG exhibited an initial drop in PCE with a stable output afterward. PCE values returned to the initial level after the break without light exposure. This effect is common in standard solar cells. It is attributed to the increase in operational temperature (as shown in Figure S10), and the drop is typically recoverable, as also observed here. For TQDG, the temperature reached ∼40 °C at the glass surface under operation conditions, indicating good thermal stability for device operation. The photostability test demonstrates that Si QD-based TQDG shows no long-term degradation trends,

https://doi.org/10.1021/acsphotonics.2c00633
ACS Photonics 2022, 9, 2499−2509

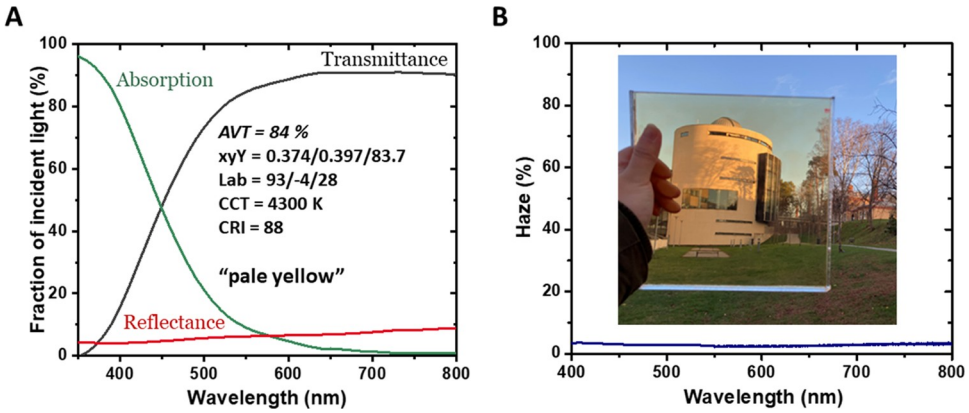

Figure 3. Aesthetic quality of TQDGs. (A) Aesthetic quality of TQDG-*l*-10, with measured transmittance spectrum (black), reflectance spectrum (red), and derived absorption spectrum (green). (B) Measured haze spectrum of TQDG-*l*-10. The inserted photo was taken with the device in an outdoor environment, demonstrating good visual characteristics of the TQDG.

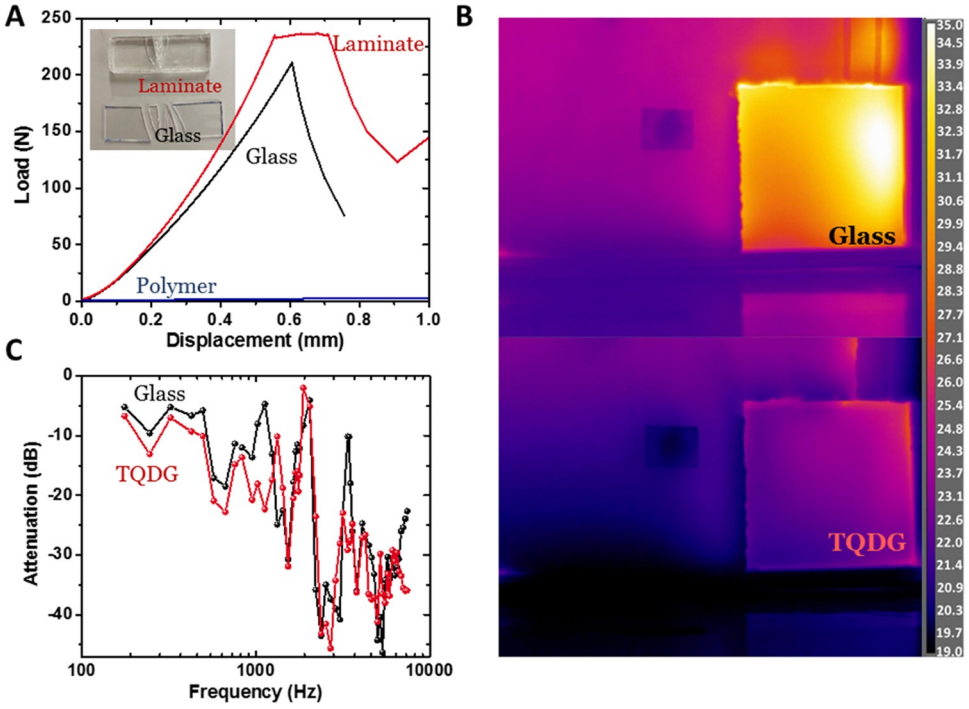

Figure 4. Mechanical and insulation properties as building envelope materials. (A) Load versus displacement for glass (black) and the laminated sample (red), with an inserted photo of the samples after breakage. (B) Last frames of the ∼15 min long movie sequence for recording the temperature evolution of the thermal box with glass (top) and the TQDG-*l*-no-QDs sample (bottom) by a thermal imaging camera. (C) Sound attenuation spectra for glass (black) and the TQDG-*l*-no-QD samples (red).

which can be ascribed to the inorganic nature of nanoparticles and proper encapsulation of the polymer composite in a triplex laminate. Standard aging tests, such as IEC 61215 for photovoltaic devices, will be performed at the next stage after complete device encapsulation in a frame, further protecting edge solar cells.

Building Envelope Material. *Aesthetic Quality.* Here, the aesthetic quality of the TQDGs is evaluated in three aspects: AVT, color rendering, and haze. All were assessed from the measured transmittance and reflectance spectra (Supporting Information 1, S4 and S5).

Due to strong UV light absorption and low absorption in the visible range, our Si QD-TQDGs exhibit high AVT values between 74 and 89%, as shown in Figures 3A and S11. Thus, such devices can indeed be placed in the category of TPV,[19] where basic visual comfort is of higher priority. Haze can also affect the visual clarity of TQDGs, where high values dramatically lower the visual characteristics and reduce the conversion efficiency due to scattering. Except for the small device with a high loading (TQDG-*s*-6-H; Figure S12), the haze in the visible range here was controlled below 3%, even for the thickest sample (∼3% for TQDG-*l*-10; Figure 3B). As a demonstration, the inserted photograph in Figure 3B confirms that the visual perception of distant objects was not affected.

With regard to color rendering, the BIPV community tends to use parameters, such as correlated color temperature (CCT) and color rendering index (CRI), to assess the visual comfort of semitransparent colored BIPV.[8] The recommended CCT for transmitted sunlight is from 3000 to 5300 K (i.e., warm and intermediate white lights), and CRI > 90 is considered ideal.

https://doi.org/10.1021/acsphotonics.2c00633
ACS Photonics 2022, 9, 2499−2509

As shown in Figure 2A, the calculated CCT and CIE-CRI values (calculated based on AM1.5G[68]) for TQDG-*l*-10 were 4300 K and 88, respectively, demonstrating that the light transmitted by these devices renders colors well, both under artificial illuminants and ambient daylight, as seen in the inserted photo in Figure 3B. CIELAB (L^*, a^*, b^*) coordinates are also commonly used for color assessment, providing additional information on appearance under one sun. The CIELAB coordinates of TQDG-*l*-10 were (93, −4, 28), and this color was then defined as a "pale yellow" (Colorhexa). This slightly deviates from the neutral/gray color definition: $0 < a^*, b^* < 15$. Although a color-neutral glass is generally preferred, aesthetic perception is often based on individual preferences. In fact, several research works showed that a warmer tinted color with a high b^* value, such as bronze, actually improves visual pleasantness and comfort to individuals, being preferred even to the neutral color.[73,74]

Mechanical Strength. For a building envelope, mechanical strength and safety are of utmost importance. To be suitable material for a window, the glass/composite should not only afford the basic service loading but also guarantee safety at failures. These characteristics are subject to numerous standards, such as EN14449. Generally, laminated glass is a popular alternative to normal float glass due to improved mechanical properties and safe postfailure behavior. During the occurrence of breakage, crack propagation is limited in laminated glass thanks to the existence of a polymer interlayer, which also keeps glass shards together in the frame. Here, we demonstrate that as a type of laminated glass, our LSC structure can provide an improved safety warrant.

The results of a three-point bending test are shown in Figure 4A. The laminate showed slightly larger load capacity with improved bending stiffness (steeper slope of the curve) compared to the single sheet glass and, more importantly, prolonged the fracture event after maximum load. The laminate did not completely fracture as the OSTE polymer material kept the structural integrity, which allowed for further displacement. As shown by the inserted photo in Figure 4A, normal glass was shattered after breakage, while our laminate sample stayed in one piece, and no dangerous debris formed. Consequently, we have proven that a triplex TQDG with a laminate structure has better toughness (area under the force−displacement curve) than normal glass, which is often used as a substrate for TQDG films. This function comes without any penalty to the photovoltaic and photo-optical performances reported above. Note that the neat OSTE polymer material itself lacks any stiffness (E-modulus is ∼1 GPa,[75] as opposite to ∼70 GPa for glass) and cannot be directly utilized for this application (blue curve in Figure 4A).

Insulation Property. Additionally, an insulation function of windows should be treated as one of the key features of indoor climate, where thermal insulation can also contribute to the reduction of building energy consumption. To test the heat insulation property of the TQDG, a thermally insulating wooden box was built and a TQDG was embedded in the wall. Then, the box interior was heated, and the temperature evolution of the TQDG and the surrounding wall was monitored by a thermal imaging camera (Supporting Information 1, S7a). A reference sample, composed of two pieces of glass clamped together, was also tested. As demonstrated in Figure 4B, the difference in the heating rate between the two kinds of samples became quickly obvious. At the end of ∼15 min long exposure for the TQDG (bottom), the temperature in the middle of the sample was <24 °C, which was barely different from the ambient. For the reference sample (top), however, it already exceeded 31 °C. The thermal conductivity of the TQDG was also quantified by stationary measurements (detailed in Supplementary S7b). The obtained value for the TQDG was around 0.2 $W{\cdot}m^{-1}{\cdot}K^{-1}$, which is 4−5 times lower than that of a normal low iron soda-lime glass (0.94 $W{\cdot}m^{-1}{\cdot}K^{-1}$). Our measured value already approaches that of standard heat insulators used in construction, such as polystyrene foams (0.06 $W{\cdot}m^{-1}{\cdot}K^{-1}$). Due to the amorphous morphology of the polymer chain, vibrational modes in the polymer tend to be localized, resulting in a low thermal conductivity. In the TQDG device, there is a thick polymer interlayer, which contributes to a small thermal conductivity of the TQDG. When recalculated to the sample thermal resistance for TQDG, it is about 20 times larger than for pristine glass, contributing to more than 30% of the total thermal resistance (Supporting Information S7c). So, a substantially higher level of thermal insulation for this TQDG configuration has been demonstrated here without sacrificing other characteristics.

Sound insulation of the building envelope can also strongly influence perceived quality. To test sound isolation of the TQDG, in comparison with glass, a sweep of audible frequencies was generated by a speaker and recorded by a microphone behind the wall with embedded samples, as above. Data are shown in Figure 4C, where the sound intensity attenuation for each case is presented in relation to the signal without a sample. Attenuation was clearly stronger in the case of LSC, especially pronounced at low and high frequencies. Some resonances, such as at ∼1 and ∼3 kHz, were also suppressed. Other transmission resonances, such as at ∼2 kHz, however, persisted. As a measure of the total attenuation, a response to "pink" noise (same amount of power in each octave) was evaluated. Integration of the measured attenuation with a pink noise spectrum reveals that for TQDG the total attenuation is two times stronger than for glass, confirming that the present TQDG configuration can offer better sound insulation for building envelopes.

State-of-the-Art. We can compare the present Si QD TQDG with other state-of-the-art TPV devices, considering that good photovoltaic performance and high aesthetic quality are both important. As mentioned above, LUE from devices with the same dimensions can be applied in semitransparent TPVs for a fair comparison between different systems.

First, in comparison with devices based on the LSC technology, here the highest LUE for the 9 × 9 cm^2 TQDGs is 0.84%, which is slightly lower than the best LUE value of 0.97% for a 10 × 10 cm^2 QD-LSC devices.[32] For devices with a dimension of 20 × 20 cm^2, the highest LUE for our TQDGs applied to a real situation (with back-reflection) was 1.3%, which is already higher than that of the highly efficient LSC-PVs based on organic dyes (1.19% for a dimension of 20 × 20 cm^2 with back-reflection)[23] and $CuInS_2$ QDs (0.9 for a dimension of 15.24 × 15.24 cm^2 with back-reflection),[50] as shown in Table S5. The high LUE value for our TQDGs, especially with a back-reflector, can be attributed to the strong light absorption in the blue and UV regions and relatively weak absorption in the remaining visible, rendering an overall high efficiency of light utilization. Despite high transparency, as demonstrated by the video in Supporting Information 2, our fabricated TQDG can indeed power an electrical device requiring a 0.1−0.2 A operating current. Simultaneously, a

https://doi.org/10.1021/acsphotonics.2c00633
ACS Photonics 2022, 9, 2499−2509

clear visual rendering of the object was provided under ambient conditions, rendering devices presented here superior, when compared to LSC-based state-of-the-art analogues.

Next, compared to TPVs based on thin film technologies, the reported PCE values in those are typically higher. Nevertheless, most of those reports are based on the very small active size of the devices (<1 cm^2), which is far from practical applications (Table S6). In addition, although some of the transparent solar cells have high LUE values, AVT values are usually well below 50%, which is also not directly applicable for solar windows. For the semitransparent PV technology, on the other hand, amorphous Si modules with a size >1 m^2 can reach a PCE of 6−7%, however, still with very low AVT values (10−20%).[76,77] So, again, when size, visible light transmittance, and efficiency are equally considered, the TQDG concept demonstrated here appears advantageous.

As for the mechanical strength and insulation properties, to the best of our knowledge, very few works, which focus on improvement in TPV performance, have considered these factors.[61] In particular, when LSC-PV types of devices are fabricated by drop-casting or doctor-blading on a glass substrate,[18,19] or even the device is just a sheet of plastic film,[23] the mechanical strength and insulation properties may be similar or even inferior to the normal glass, thus lacking required strengths and isolation properties. If a combination with other functional glass sheets in a window module is considered, those additions may, in turn, detrimentally affect efficiency and aesthetical characteristics reported for a single sheet. In contrast, our TQDG devices already exhibit improved mechanical strengths and insulation properties than normal floating glass, benefiting from the triplex laminate configuration. A proper new metric, in which all of these factors are combined, should be devised and used for reporting different prototypes to facilitate fair comparison.

CONCLUSIONS

In summary, large-area TQDGs based on Si QDs were fabricated, with balanced PV performance and aesthetic quality. By optimizing the interlayer thickness and QD loading in the devices, our prototype TQDG with dimensions of 20 × 20 cm^2 can deliver a PCE of up to 1.57% with a back-reflector, featuring at the same time a very high transmittance of >80%. In addition to the energy generation aspect, this material also possesses good thermal insulation, which can further improve energy efficiency in buildings when applied as an envelope material. Stronger mechanical and sound insulation properties compared to bare glass/plastic were also shown. Thus, we demonstrated that a material system based on environmentally friendly Si nanocrystals is promising for functional semitransparent photovoltaics. Further improvement in the PV performance of such TQDGs could be realized by enhancing the PLQY of the QD/polymer nanocomposite and extending the absorption of such TQDGs with a complementary nanophosphor. In addition, low cost and scalable fabrication of TQDGs also need to be addressed for their future commercialization. We stress that a thorough comparison between different TQDG designs and material systems should be carried out by taking into account not only photo-optical and photovoltaic characteristics but also including relevant aspects of device size and the functional material for building integration.

EXPERIMENTAL SECTION

Fabrication of TQDG. *Synthesis of Si QDs.* A commercial hydrogen silsesquioxane (HSQ) powder from Applied Quantum Materials Inc. (Canada) was annealed at 1200 °C in a 5% H_2 and 95% Ar atmosphere for 1 h, resulting in the formation of a black Si QDs/SiO_2 powder. To efficiently release Si QDs from the SiO_2 matrix during the etching process, the obtained Si QDs/SiO_2 powder was first ground with a mortar and pestle, followed by shaking in ethanol. For etching away the SiO_2 matrix, 200 mg of the fine Si QDs/SiO_2 powder was mixed with 5 mL of ethanol and 5 mL of DI water in a polypropylene centrifuge tube under magnetic stirring. A 50% aqueous hydrofluoric acid (HF) solution (5 mL) was then slowly added to the mixture under stirring. *Caution: HF solution is extremely dangerous, and specific safety equipment is necessary for operation.* The suspension turned yellow after stirring for 1 h, indicating that the Si QDs were released from the SiO_2 matrix. The resulting hydride-terminated nanoparticles were collected by extractions with 10 mL of toluene twice, followed by centrifugation at 11 000 rpm for 10 min. The precipitate was then collected for surface passivation.

For surface passivation, the fresh hydride-terminated Si QDs were mixed with 6 mL of methyl 10-undecenoate (Sigma-Aldrich, 96%) and the mixture was sonicated for 5 min to get homogeneous wetting. Then, the suspension was loaded in a flask and transferred to an argon-charged Schlenk line. The reaction mixture was kept at 190 °C for 19 h under an Ar atmosphere, and the brown suspension changed to a clear orange/brown solution, which was stored directly for further application. To obtain the Si QD powder, 1.5 mL of hexane was first added to 0.5 mL of Si QD ester solution, and then the suspension was centrifuged at 8000 rpm for 5 min to separate Si QDs from the liquid phase. Finally, the supernatant was discarded, and the resulting Si QDs were used for fabricating nanocomposites directly.

Fabrication of TQDG Based on Si QD/OSTE Nanocomposites. The thiol monomers were pentaerythritol tetrakis (3-mercaptobutylate), and the allyl monomers were triallyl-1,3,5-triazine-2,4,6 (1H,3H,5H)-trione. Both of them were from Mercene Labs AB, Sweden, as well as the photoinitiator (1-hydroxycyclohexyl phenyl ketone, Irgacure-184). For the standard preparation of the nanocomposite with a QD loading of 0.05% by weight, 2 mg of Si QD powder was dispersed in 0.96 g of allyl monomers first, giving a clear orange solution, and then 3.11 g of thiol monomers (to obtain a thiol/allyl group ratio of 2/1) and 0.04 g of initiator were added to the solution. For samples with other QD loadings, the amount of Si QDs was changed accordingly. Then, the mixture was sonicated for 10 min for thorough mixing and finally placed in an evacuated desiccator to remove air bubbles from the solution. The homogeneous solution was slowly poured into a prepared glass box (made by borosilicate glass) and cured with 360 nm light from a UV torch for 30 s to trigger the thiol−ene polymerization reaction. To obtain a uniform nanocomposite interlayer, the intensity of UV light was kept below 0.1 mW/cm^2. A slow layer-by-layer polymerization was applied to reduce the final polymer shrinkage and minimize the formation of debonding gaps.

After the polymerization finished, commercial monocrystalline Si solar cells (IXYS, IXOLAR, SM141K08L, 88 × 15 mm^2) were directly coupled to the edges of the QD-laminated glass by a commercial glass glue, with the excess part covered

https://doi.org/10.1021/acsphotonics.2c00633
ACS Photonics 2022, 9, 2499−2509

by black tapes. All solar cells were connected in parallel before being attached to the devices. The detailed device fabrication procedure can be found in Supporting Information 1, S2b.

Optical Measurements. UV−vis absorption spectra of Si QD solution were collected on a Lambda 750 UV−vis spectrophotometer. Photoluminescence spectra and absolute PLQY were measured in a homebuilt integrating sphere setup. Transmittance and haze measurements of TQDG were conducted by following the standard test method for haze and luminous transmittance of transparent plastics (D1003-00). A light source, integrating sphere, and signal acquisition system used here was the same as in the PLQY measurements (for details, see Supporting Information 1, S4).

Photovoltaic Measurements. The photovoltaic performance of the TQDGs was investigated using a large-area LED-based solar simulator (Sunbrick from G2V optics, 350−1100 nm spectral range, ASTM E927 class AAA+, 25 × 25 cm^2) and carried out by applying an external potential bias (from 0 to 6 V) to the device while recording the generated photocurrent with a Keithley model 2450 digital source meter. Excess parts on the solar cells were covered by black tape. For the TQDG-*l* series, two solar cells were connected in parallel before being attached to one edge of the device. All other three edges, which were not coupled with solar cells, were painted black to eliminate reflection there. For the device of TQDG-*l*-10, *I*−*V* measurements were also performed when the edges were fully covered by solar cells, which all were connected in parallel. In addition, an opaque mask with a width of 5 mm was placed on top of the solar cells to block direct illumination to the solar cells. For the *I*−*V* measurements with a back-reflector, a white paper was placed beneath the TQDGs at a distance of 6 cm.

For the devices with one edge coupled with solar cells, PCE values of the TQDGs were calculated using

$$\mathrm{PCE} = \frac{I_{sc} \cdot V_{oc} \cdot \mathrm{FF} \cdot 4}{I_0 \cdot A_{top}} \quad (4)$$

where I_{sc}, V_{oc}, and FF were obtained directly from the measured *I*−*V* curves, I_0 is the light intensity of AM1.5 G, which is 0.1 W/cm^2, and A_{top} is the surface area of the TQDGs.

For TQDG-*l*-10 with four edges coupled by solar cells, its PCE value was calculated by

$$\mathrm{PCE} = \frac{I_{sc} \cdot V_{oc} \cdot \mathrm{FF}}{I_0 \cdot A_{top}} \quad (5)$$

EQE measurements were performed on the same samples as those for *I*−*V* measurements, i.e., with blackened edges and blocked direct illumination. Monochromatic light was obtained from each single LED channel of the same large-area solar simulator, and the intensity was calibrated by a thermal power meter. For each monochromatic light used in EQE measurements, a set of LEDs with the same light wavelength were switched on, giving rather uniform illumination on the whole TQDG device. The photocurrent was recorded by the same source meter. EQE values were obtained by dividing the number of electrons from the short circuit current by the number of solar photons impinging on the TQDG top surface for each wavelength.

Mechanical Tests and Thermal Conductivity Measurements. A three-point bending measurement was carried out to test the mechanical property of laminates, conducted in a universal testing machine (Instron 5566, UK) with a load cell capacity of 10 kN, and the support span was 40 mm. The piston speed was 1 mm/min for the tests. The thermal insulation property of the TQDG was evaluated by both a Thermal imaging camera (FLIR A600 series, 640 × 480 pixels, object temperature range from −20 to 150 °C) and thermocouples (for details, see Supporting Information 1, S7).

■ ASSOCIATED CONTENT

Supporting Information

The Supporting Information is available free of charge at https://pubs.acs.org/doi/10.1021/acsphotonics.2c00633.

Supporting Information 1: power conversion efficiency formula, detailed procedure of TQDG fabrication, photovoltaic and optical measurement results for other TQDGs, details for mechanical and thermal conductivity measurements, and summary of literature reports (PDF)

Supporting Information 2 is a video showing that a TQDG is powering an electrical device while maintaining good visual perception of the object (MP4)

■ AUTHOR INFORMATION

Corresponding Author

Ilya Sychugov − *Department of Applied Physics, KTH Royal Institute of Technology, Stockholm 114 19, Sweden;* orcid.org/0000-0003-2562-0540; Email: ilyas@kth.se

Authors

Jing Huang − *Department of Applied Physics, KTH Royal Institute of Technology, Stockholm 114 19, Sweden;* orcid.org/0000-0001-6005-2302

Jingjian Zhou − *Department of Applied Physics, KTH Royal Institute of Technology, Stockholm 114 19, Sweden;* orcid.org/0000-0002-6623-2491

Erik Jungstedt − *Department of Fiber and Polymer Technology, KTH Royal Institute of Technology, Stockholm 100 44, Sweden*

Archana Samanta − *Department of Applied Physics, KTH Royal Institute of Technology, Stockholm 114 19, Sweden*

Jan Linnros − *Department of Applied Physics, KTH Royal Institute of Technology, Stockholm 114 19, Sweden*

Lars A. Berglund − *Department of Fiber and Polymer Technology, KTH Royal Institute of Technology, Stockholm 100 44, Sweden;* orcid.org/0000-0001-5818-2378

Complete contact information is available at: https://pubs.acs.org/10.1021/acsphotonics.2c00633

Funding

This work was supported by Swedish Energy Agency (46360-1).

Notes

The authors declare no competing financial interest.

■ ACKNOWLEDGMENTS

J.Z. acknowledges support from the China Scholarship Council (CSC).

■ REFERENCES

(1) Lee, K.; Um, H. D.; Choi, D.; Park, J.; Kim, N.; et al. The Development of Transparent Photovoltaics. *Cell Rep. Phys. Sci.* **2020**, *1*, No. 100143.

(2) Lee, H.; Song, H. J. Current status and perspective of colored photovoltaic modules. *WIREs Energy Environ.* **2021**, *10*, No. e403.

(3) Li, Z.; Ma, T.; Yang, H.; Lu, L.; Wang, R. Transparent and Colored Solar Photovoltaics for Building Integration. *Sol. RRL* **2021**, *5*, No. 2000614.
(4) Debije, M. G.; Verbunt, P. P. C. Thirty Years of Luminescent Solar Concentrator Research: Solar Energy for the Built Environment. *Adv. Energy Mater.* **2012**, *2*, 12−35.
(5) Traverse, C. J.; Pandey, R.; Barr, M. C.; Lunt, R. R. Emergence of highly transparent photovoltaics for distributed applications. *Nat. Energy* **2017**, *2*, 849−860.
(6) Meinardi, F.; Bruni, F.; Brovelli, S. Luminescent solar concentrators for building-integrated photovoltaics. *Nat. Rev. Mater.* **2017**, *2*, 17072.
(7) Needell, D. R.; Phelan, M. E.; Hartlove, J. T.; Atwater, H. A. Solar power windows: Connecting scientific advances to market signals. *Energy* **2021**, *219*, No. 119567.
(8) Eder Gabriele, P. G.; Trattnig, R.; Bonomo, P.; Saretta, E.; Frontini, F. et al. Colored BIPV, Market, Research and Development *IEA PVPS*, 2019, *T15-07*, 2019.
(9) Sutherland, B. R. Sunshine through the Looking Glass. *Joule* **2018**, *2*, 1657−1658.
(10) Lee, K.; Kim, N.; Kim, K.; Um, H. D.; Jin, W.; et al. Neutral-Colored Transparent Crystalline Silicon Photovoltaics. *Joule* **2020**, *4*, 235−246.
(11) Franklin, E.; Everett, V.; Blakers, A.; Weber, K. Sliver Solar Cells: High-Efficiency, Low-Cost PV Technology. *Adv. OptoElectron.* **2007**, *2007*, No. 035383.
(12) Burgués-Ceballos, I.; Lucera, L.; Tiwana, P.; Ocytko, K.; Tan, L. W.; et al. Transparent organic photovoltaics: A strategic niche to advance commercialization. *Joule* **2021**, *5*, 2261−2272.
(13) Chen, C. C.; Dou, L.; Zhu, R.; Chung, C. H.; Song, T. B.; et al. Visibly Transparent Polymer Solar Cells Produced by Solution Processing. *ACS Nano* **2012**, *6*, 7185−7190.
(14) Liu, Q.; Gerling, L. G.; Bernal Texca, F.; Toudert, J.; Li, T.; et al. Light Harvesting at Oblique Incidence Decoupled from Transmission in Organic Solar Cells Exhibiting 9.8% Efficiency and 50% Visible Light Transparency. *Adv. Energy Mater.* **2020**, *10*, No. 1904196.
(15) Liu, D.; Yang, C.; Lunt, R. R. Halide Perovskites for Selective Ultraviolet-Harvesting Transparent Photovoltaics. *Joule* **2018**, *2*, 1827−1837.
(16) Xue, Q.; Xia, R.; Brabec, C. J.; Yip, H. L. Recent advances in semi-transparent polymer and perovskite solar cells for power generating window applications. *Energy Environ. Sci.* **2018**, *11*, 1688−1709.
(17) Rafiee, M.; Chandra, S.; Ahmed, H.; McCormack, S. J. An overview of various configurations of Luminescent Solar Concentrators for photovoltaic applications. *Opt. Mater.* **2019**, *91*, 212−227.
(18) Yang, C.; Moemeni, M.; Bates, M.; Sheng, W.; Borhan, B.; Lunt, R. R. High-Performance Near-Infrared Harvesting Transparent Luminescent Solar Concentrators. *Adv. Opt. Mater.* **2020**, *8*, No. 1901536.
(19) Yang, C.; Sheng, W.; Moemeni, M.; Bates, M.; Herrera, C. K.; et al. Ultraviolet and Near-Infrared Dual-Band Selective-Harvesting Transparent Luminescent Solar Concentrators. *Adv. Energy Mater.* **2021**, *11*, No. 2003581.
(20) Weber, W. H.; Lambe, J. Luminescent greenhouse collector for solar radiation. *Appl. Opt.* **1976**, *15*, 2299−2300.
(21) Goetzberger, A.; Greube, W. Solar energy conversion with fluorescent collectors. *Appl. Phys.* **1977**, *14*, 123−139.
(22) Goetzberger, A.; Wittwer, V. Fluorescent planar collector-concentrators: A review. *Sol. Cells* **1981**, *4*, 3−23.
(23) Zhang, B.; Zhao, P.; Wilson, L. J.; Subbiah, J.; Yang, H.; et al. High-Performance Large-Area Luminescence Solar Concentrator Incorporating a Donor−Emitter Fluorophore System. *ACS Energy Lett.* **2019**, *4*, 1839−1844.
(24) Slooff, L. H.; Bende, E. E.; Burgers, A. R.; Budel, T.; Pravettoni, M.; et al. A luminescent solar concentrator with 7.1% power conversion efficiency. *Phys. Status Solidi RRL* **2008**, *2*, 257−259.
(25) Mateen, F.; Li, Y.; Saeed, M. A.; Sun, Y.; Zhang, Y.; et al. Large-area luminescent solar concentrator utilizing donor-acceptor luminophore with nearly zero reabsorption: Indoor/outdoor performance evaluation. *J. Lumin.* **2021**, *231*, No. 117837.
(26) Corsini, F.; Nitti, A.; Tatsi, E.; Mattioli, G.; Botta, C.; et al. Large-Area Semi-Transparent Luminescent Solar Concentrators Based on Large Stokes Shift Aggregation-Induced Fluorinated Emitters Obtained Through a Sustainable Synthetic Approach. *Adv. Opt. Mater.* **2021**, *9*, No. 2100182.
(27) Huang, J.; Zhou, J.; Haraldsson, T.; Clemments, A.; Fujii, M.; et al. Triplex Glass Laminates with Silicon Quantum Dots for Luminescent Solar Concentrators. *Sol. RRL* **2020**, *4*, No. 2000195.
(28) Wu, K.; Li, H.; Klimov, V. I. Tandem luminescent solar concentrators based on engineered quantum dots. *Nat. Photonics* **2018**, *12*, 105−110.
(29) Meinardi, F.; Ehrenberg, S.; Dhamo, L.; Carulli, F.; Mauri, M.; et al. Highly efficient luminescent solar concentrators based on earth-abundant indirect-bandgap silicon quantum dots. *Nat. Photonics* **2017**, *11*, 177−185.
(30) Meinardi, F.; Colombo, A.; Velizhanin, K. A.; Simonutti, R.; Lorenzon, M.; et al. Large-area luminescent solar concentrators based on 'Stokes-shift-engineered' nanocrystals in a mass-polymerized PMMA matrix. *Nat. Photonics* **2014**, *8*, 392−399.
(31) Zhao, H.; Liu, G.; You, S.; Camargo, F. V. A.; Zavelani-Rossi, M.; et al. Gram-scale synthesis of carbon quantum dots with a large Stokes shift for the fabrication of eco-friendly and high-efficiency luminescent solar concentrators. *Energy Environ. Sci.* **2021**, *14*, 396−406.
(32) Bergren, M. R.; Makarov, N. S.; Ramasamy, K.; Jackson, A.; Guglielmetti, R.; McDaniel, H. High-Performance CuInS2 Quantum Dot Laminated Glass Luminescent Solar Concentrators for Windows. *ACS Energy Lett.* **2018**, *3*, 520−525.
(33) Sadeghi, S.; Bahmani Jalali, H.; Srivastava, S. B.; Melikov, R.; Baylam, I.; et al. High-Performance, Large-Area, and Ecofriendly Luminescent Solar Concentrators Using Copper-Doped InP Quantum Dots. *iScience* **2020**, *23*, No. 101272.
(34) Chen, W.; Li, J.; Liu, P.; Liu, H.; Xia, J.; et al. Heavy Metal Free Nanocrystals with Near Infrared Emission Applying in Luminescent Solar Concentrator. *Sol. RRL* **2017**, *1*, No. 1700041.
(35) Liu, G.; Mazzaro, R.; Wang, Y.; Zhao, H.; Vomiero, A. High efficiency sandwich structure luminescent solar concentrators based on colloidal quantum dots. *Nano Energy* **2019**, *60*, 119−126.
(36) Meinardi, F.; Akkerman, Q. A.; Bruni, F.; Park, S.; Mauri, M.; et al. Doped Halide Perovskite Nanocrystals for Reabsorption-Free Luminescent Solar Concentrators. *ACS Energy Lett.* **2017**, *2*, 2368−2377.
(37) Li, Z.; Johnston, A.; Wei, M.; Saidaminov, M. I.; Martins de Pina, J.; et al. Solvent-Solute Coordination Engineering for Efficient Perovskite Luminescent Solar Concentrators. *Joule* **2020**, *4*, 631−643.
(38) Wei, M.; de Arquer, F. P. G.; Walters, G.; Yang, Z.; Quan, L. N.; et al. Ultrafast narrowband exciton routing within layered perovskite nanoplatelets enables low-loss luminescent solar concentrators. *Nat. Energy* **2019**, *4*, 197−205.
(39) Cai, K.-B.; Huang, H. Y.; Chen, P. W.; Wen, X.; Li, K.; et al. Highly transparent and luminescent gel glass based on reabsorption-free gold nanoclusters. *Nanoscale* **2020**, *12*, 10781−10789.
(40) Huang, H. Y.; Cai, K.; Chen, P. W.; Lin, C. A. J.; Chang, S. H.; Yuan, C. T. Engineering Ligand−Metal Charge Transfer States in Cross-Linked Gold Nanoclusters for Greener Luminescent Solar Concentrators with Solid-State Quantum Yields Exceeding 50% and Low Reabsorption Losses. *J. Phys. Chem. C* **2018**, *122*, 20019−20026.
(41) Roncali, J. Luminescent Solar Collectors: Quo Vadis? *Adv. Energy Mater.* **2020**, *10*, No. 2001907.
(42) Debije, M. G.; Evans, R. C.; Griffini, G. Laboratory protocols for measuring and reporting the performance of luminescent solar concentrators. *Energy Environ. Sci.* **2021**, *14*, 293−301.
(43) Hill, S. K. E.; Connell, R.; Held, J.; Peterson, C.; Francis, L.; et al. Poly(methyl methacrylate) Films with High Concentrations of

https://doi.org/10.1021/acsphotonics.2c00633
ACS Photonics 2022, 9, 2499−2509

Silicon Quantum Dots for Visibly Transparent Luminescent Solar Concentrators. *ACS Appl. Mater. Interfaces* **2020**, *12*, 4572−4578.
(44) Zhou, Y.; Benetti, D.; Fan, Z.; Zhao, H.; Ma, D.; et al. Near Infrared, Highly Efficient Luminescent Solar Concentrators. *Adv. Energy Mater.* **2016**, *6*, No. 1501913.
(45) Bomm, J.; Büchtemann, A.; Chatten, A. J.; Bose, R.; Farrell, D. J.; et al. Fabrication and full characterization of state-of-the-art quantum dot luminescent solar concentrators. *Sol. Energy Mater. Sol. Cells* **2011**, *95*, 2087−2094.
(46) van Sark, W.; Moraitis, P.; Aalberts, C.; Drent, M.; Grasso, T.; et al. The "Electric Mondrian" as a Luminescent Solar Concentrator Demonstrator Case Study. *Solar RRL* **2017**, *1*, No. 1600015.
(47) Kanellis, M.; de Jong, M. M.; Slooff, L.; Debije, M. G. The solar noise barrier project: 1. Effect of incident light orientation on the performance of a large-scale luminescent solar concentrator noise barrier. *Renewable Energy* **2017**, *103*, 647−652.
(48) Debije, M. G.; Tzikas, C.; Rajkumar, V. A.; de Jong, M. M. The solar noise barrier project: 2. The effect of street art on performance of a large scale luminescent solar concentrator prototype. *Renewable Energy* **2017**, *113*, 1288−1292.
(49) Vossen, F. M.; Aarts, M. P. J.; Debije, M. G. Visual performance of red luminescent solar concentrating windows in an office environment. *Energy Build.* **2016**, *113*, 123−132.
(50) Velarde, A. R. M.; Bartlett, E. R.; Makarov, N. S.; Castañeda, C.; Jackson, A.; et al. Optimizing the Aesthetics of High-Performance CuInS2/ZnS Quantum Dot Luminescent Solar Concentrator Windows. *ACS Appl. Energy Mater.* **2020**, *3*, 8159−8163.
(51) Anand, A.; Zaffalon, M. L.; Gariano, G.; Camellini, A.; Gandini, M.; et al. Evidence for the Band-Edge Exciton of CuInS2 Nanocrystals Enables Record Efficient Large-Area Luminescent Solar Concentrators. *Adv. Funct. Mater.* **2020**, *30*, No. 1906629.
(52) Meinardi, F.; McDaniel, H.; Carulli, F.; Colombo, A.; Velizhanin, K. A.; et al. Highly efficient large-area colourless luminescent solar concentrators using heavy-metal-free colloidal quantum dots. *Nat. Nanotechnol.* **2015**, *10*, 878−886.
(53) Li, H.; Wu, K.; Lim, J.; Song, H. J.; Klimov, V. I. Doctor-blade deposition of quantum dots onto standard window glass for low-loss large-area luminescent solar concentrators. *Nat. Energy* **2016**, *1*, 16157.
(54) Mazzaro, R.; Gradone, A.; Angeloni, S.; Morselli, G.; Cozzi, P. G.; et al. Hybrid Silicon Nanocrystals for Color-Neutral and Transparent Luminescent Solar Concentrators. *ACS Photonics* **2019**, *6*, 2303−2311.
(55) Han, S.; Chen, G.; Shou, C.; Peng, H.; Jin, S.; Tu, C. C. Visibly Transparent Solar Windows Based on Colloidal Silicon Quantum Dots and Front-Facing Silicon Photovoltaic Cells. *ACS Appl. Mater. Interfaces* **2020**, *12*, 43771−43777.
(56) Marinins, A.; Zandi Shafagh, R.; van der Wijngaart, W.; Haraldsson, T.; Linnros, J.; et al. Light-Converting Polymer/Si Nanocrystal Composites with Stable 60−70% Quantum Efficiency and Their Glass Laminates. *ACS Appl. Mater. Interfaces* **2017**, *9*, 30267−30272.
(57) Zhou, J.; Huang, J.; Chen, H.; Samanta, A.; Linnros, J.; et al. Low-Cost Synthesis of Silicon Quantum Dots with Near-Unity Internal Quantum Efficiency. *J. Phys. Chem. Lett.* **2021**, *12*, 8909−8916.
(58) Hill, S. K. E.; Connell, R.; Peterson, C.; Hollinger, J.; Hillmyer, M. A.; et al. Silicon Quantum Dot−Poly(methyl methacrylate) Nanocomposites with Reduced Light Scattering for Luminescent Solar Concentrators. *ACS Photonics* **2019**, *6*, 170−180.
(59) Foraboschi, P. Behavior and Failure Strength of Laminated Glass Beams. *J. Eng. Mech.* **2007**, *133*, 1290−1301.
(60) Biolzi, L.; Cattaneo, S.; Orlando, M.; Piscitelli, L. R.; Spinelli, P. Post-failure behavior of laminated glass beams using different interlayers. *Compos. Struct.* **2018**, *202*, 578−589.
(61) Sun, C.; Xia, R.; Shi, H.; Yao, H.; Liu, X.; et al. Heat-Insulating Multifunctional Semitransparent Polymer Solar Cells. *Joule* **2018**, *2*, 1816−1826.
(62) Chae, Y. T.; Kim, J.; Park, H.; Shin, B. Building energy performance evaluation of building integrated photovoltaic (BIPV) window with semi-transparent solar cells. *Appl. Energy* **2014**, *129*, 217−227.
(63) Ravyts, S.; Dalla Vecchia, M.; Van den Broeck, G.; Driesen, J. Review on Building-Integrated Photovoltaics Electrical System Requirements and Module-Integrated Converter Recommendations. *Energies* **2019**, *12*, 1532.
(64) Corrao, R. Mechanical Tests on Innovative BIPV Façade Components for Energy, Seismic, and Aesthetic Renovation of High-Rise Buildings. *Sustainability* **2018**, *10*, 4523.
(65) Sychugov, I. Analytical description of a luminescent solar concentrator. *Optica* **2019**, *6*, 1046−1049.
(66) Sychugov, I. Geometry effects on luminescence solar concentrator efficiency: analytical treatment. *Appl. Opt.* **2020**, *59*, 5715−5722.
(67) Yang, C.; Atwater, H. A.; Baldo, M. A.; Baran, D.; Barile, C. J.; et al. Consensus statement: Standardized reporting of power-producing luminescent solar concentrator performance. *Joule* **2022**, *6*, 8−15.
(68) Yang, C.; Liu, D.; Lunt, R. R. How to Accurately Report Transparent Luminescent Solar Concentrators. *Joule* **2019**, *3*, 2871−2876.
(69) Sefannaser, M.; Thomas, S. A.; Anderson, K. J.; Petersen, R. J.; Brown, S. L.; et al. Radiative Relaxation in Luminescent Silicon Nanocrystal Thiol-Ene Composites. *J. Phys. Chem. C* **2021**, *125*, 5824−5831.
(70) Hessel, C. M.; Henderson, E. J.; Veinot, J. G. C. Hydrogen Silsesquioxane: A Molecular Precursor for Nanocrystalline Si−SiO2 Composites and Freestanding Hydride-Surface-Terminated Silicon Nanoparticles. *Chem. Mater.* **2006**, *18*, 6139−6146.
(71) Krumer, Z.; van Sark, W. G. J. H. M.; Schropp, R. E. I.; de Mello Donegá, C. Compensation of self-absorption losses in luminescent solar concentrators by increasing luminophore concentration. *Sol. Energy Mater. Sol. Cells* **2017**, *167*, 133−139.
(72) Li, Y.; Sun, Y.; Zhang, Y. Boosting the cost-effectiveness of luminescent solar concentrators through subwavelength sanding treatment. *Sol. Energy* **2020**, *198*, 151−159.
(73) Aste, N.; Tagliabue, L. C.; Palladino, P.; Testa, D. Integration of a luminescent solar concentrator: Effects on daylight, correlated color temperature, illuminance level and color rendering index. *Sol. Energy* **2015**, *114*, 174−182.
(74) Arsenault, H.; Hébert, M.; Dubois, M. C. Effects of glazing colour type on perception of daylight quality, arousal, and switch-on patterns of electric light in office rooms. *Build. Environ.* **2012**, *56*, 223−231.
(75) Carlborg, C. F.; Haraldsson, T.; Öberg, K.; Malkoch, M.; van der Wijngaart, W. Beyond PDMS: off-stoichiometry thiol−ene (OSTE) based soft lithography for rapid prototyping of microfluidic devices. *Lab Chip* **2011**, *11*, 3136−3147.
(76) Tsai, C. Y.; Tsai, C. Y. See-through, light-through, and color modules for large-area tandem amorphous/microcrystalline silicon thin-film solar modules: Technology development and practical considerations for building-integrated photovoltaic applications. *Renewable Energy* **2020**, *145*, 2637−2646.
(77) Yeop Myong, S.; Won Jeon, S. Design of esthetic color for thin-film silicon semi-transparent photovoltaic modules. *Sol. Energy Mater. Sol. Cells* **2015**, *143*, 442−449.

https://doi.org/10.1021/acsphotonics.2c00633
ACS Photonics 2022, 9, 2499−2509